Editors' Suggestion

Optical levitation and feedback cooling of a nanoparticle at subwavelength distances from a membrane

Rozenn Diehl, Erik Hebestreit, René Reimann, Felix Tebbenjohanns, Martin Frimmer, and Lukas Novotny
ETH Zürich, Photonics Laboratory, 8093 Zürich, Switzerland

(Received 25 June 2018; published 30 July 2018)

We optically trap a nanoparticle in a laser beam strongly focused on a dielectric membrane in vacuum. By investigating the motion of the trapped particle, we map the position-dependent optical potential in front of the membrane while interferometrically measuring the distance between the particle and the membrane surface. Furthermore, we demonstrate feedback cooling of the particle's motion in subwavelength proximity to the dielectric surface. The demonstrated optomechanical control of a levitated nanoparticle in close proximity of an interface at low gas pressures is an integral requirement to investigate short-range interactions in yet unexplored parameter regimes.

DOI: 10.1103/PhysRevA.98.013851

I. INTRODUCTION

Optically levitated nanomechanical systems have emerged as an experimental platform operating at the limits set by our current understanding of physics [1,2]. The position of an optically levitated nanoparticle can be measured with a precision ultimately governed by the Heisenberg uncertainty relation of quantum mechanics [3]. This measurement precision has been harnessed to control the levitated particle's center-of-mass dynamics and feedback cool its motion towards the quantum ground state [4–8]. Furthermore, this precision is at the heart of the outstanding sensitivity of optically levitated sensing systems [9–12]. In close analogy to trapped-atom sensors [13], levitated nanoparticles are promising systems for exploring short-range forces [14–16]. Importantly, the large mass density of optically levitated nanoparticles will allow the investigation of these interactions in previously inaccessible parameter regimes [17]. Two requirements need to be met in order to unlock the potential of optically levitated nanosystems for short-range force sensing. First, a nanoparticle has to be levitated in subwavelength proximity of a material surface in vacuum. Second, the center-of-mass motion of the nanoparticle in the optical trap must be controlled to deploy protocols developed for the sensing of static forces. These protocols rely on feedback cooling [18]. So far, optical trapping of a particle next to an interface has been demonstrated in dense media, where the particle motion is strongly overdamped [19,20]. Nonetheless, despite the tantalizing opportunities, levitating a particle in close proximity of a surface and controlling such a particle's motion in vacuum has remained elusive to date.

In this paper, we controllably position an optically levitated nanoparticle at a subwavelength distance from a dielectric membrane and map the optical potential in the vicinity of this surface. As we approach the dielectric membrane to the laser focus, the oscillation frequency of the particle serves as a measure for the varying trap stiffness resulting from interference of the trapping light with its reflection from the membrane. At the same time, we interferometrically monitor the distance between surface and particle with a probe field independent of the optical trap. Furthermore, we demonstrate feedback cooling of the particle's center-of-mass motion in close proximity of the surface. Finally, we discuss how our experiments will enable the detection of short-range interactions between a nanoparticle and a dielectric surface.

II. EXPERIMENTAL SETUP

Our experimental setup is shown in Fig. 1(a). A linearly polarized laser beam (wavelength 1064 nm, focal power 120 mW) is focused by an objective ($100\times$, NA $= 0.9$) to trap a single silica nanoparticle of 136 nm diameter [21]. The laser intensity can be controlled with an electro-optic modulator (EOM). A collection lens collimates the light scattered by the particle in the forward direction. We use the balanced homodyne detection scheme (PD1) detailed in Ref. [5] to measure the particle position along all three axes (z denotes the optical axis and x the polarization direction of the trapping laser). Between particle and collection lens, we place a suspended silicon nitride (SiN) membrane (thickness $t = 500$ nm) normal to the optical axis. The membrane is mounted on a piezoelectric stage which allows us to position the membrane with nm precision relative to the focal plane of the objective. Prior to any measurement, we discharge the particle to avoid undesired electrostatic interactions with the membrane [21,22].

The relevant geometrical parameters of our experiment are illustrated in Fig. 1(b). The distance between the objective and the focal plane is fixed to 1 mm by the working distance of our objective. By moving the membrane along the optical axis, we can adjust the distance d_{foc} between the membrane's front surface and the focal plane. Importantly, back reflections from the membrane modify the optical potential, such that the trapped particle does not necessarily reside in the focal plane of the objective. We denote the distance between the particle and the membrane as d_{part}. To calibrate the distance d_{foc} between the membrane surface and the objective's focal point, we introduce a quarter-wave plate ($\lambda/4$) in the beam path before the objective. Without a particle in the trap, we scan the membrane position along the optical axis through the

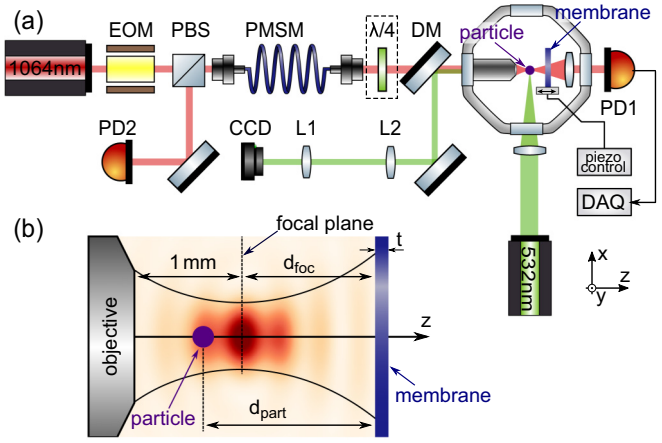

FIG. 1. (a) Experimental setup. A silica nanoparticle is trapped inside a vacuum chamber in the focus of a laser beam (1064 nm) which is spatially filtered by a polarization-maintaining single-mode fiber (PMSM). The laser beam can be modulated in intensity by an electro-optic modulator (EOM). The forward-scattered light from the nanoparticle is detected by a balanced photodetector (PD1). A SiN membrane (thickness 500 nm) is placed between the particle and the collection lens on a piezoelectric stage. To calibrate the focus-to-surface distance d_{foc}, we introduce a quarter-wave plate ($\lambda/4$) such that the light that is back reflected from the surface is deflected by the polarizing beam splitter (PBS), and reaches a photodetector (PD2). To determine the particle-to-surface distance d_{part}, a linearly polarized green laser (532 nm, 80 mW) is weakly focused on the nanoparticle and the back focal plane of the objective is imaged onto a camera (CCD) using lenses L1 and L2 and the dichroic mirror (DM). (b) Illustration of relevant geometrical parameters (not to scale). The distance d_{foc} between the focal plane of the objective and the front surface of the SiN membrane (nominal thickness $t = 500$ nm) can be adjusted by moving the membrane with the piezostage. The optical potential (illustrated by the red intensity distribution) results from the focused laser beam interfering with its own reflection at the membrane and determines the distance d_{part} between the particle and the membrane surface.

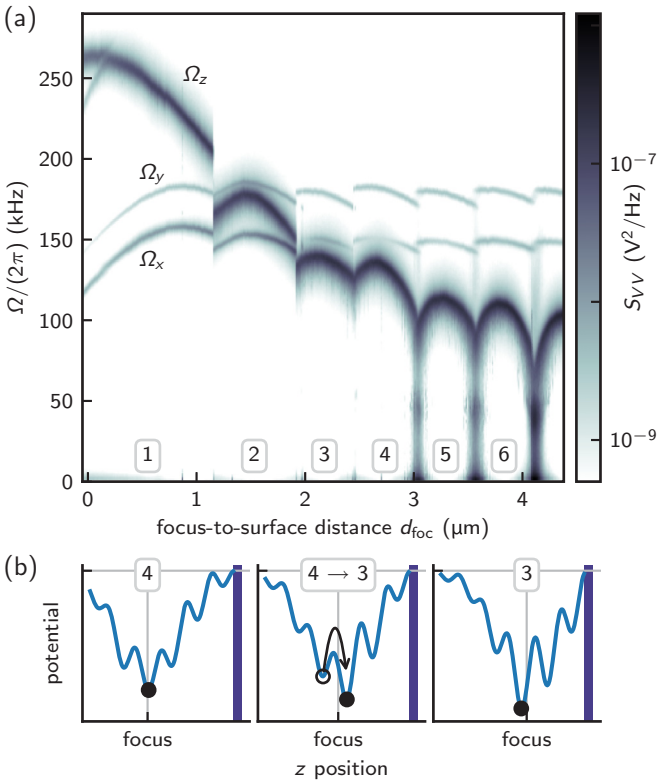

FIG. 2. (a) Measured power spectral density of the center-of-mass motion of the nanoparticle, for varying focus-to-surface distances d_{foc}. The strong feature in each spectrum is the eigenmode of the particle's center-of-mass motion along the z axis with frequency Ω_z. The two weaker features at Ω_x and Ω_y correspond to oscillations along the transverse directions (parallel to the surface), at around 150 and 175 kHz, respectively. (b) Sketches of the optical potential along the optical axis illustrating the particle's transition from potential well 4 to well 3. The wells are generated by interference of the incoming trapping laser with its reflection at the membrane. We number the wells starting with the one closest to the interface. Left: The particle is in well 4. Middle: After approaching the surface, the potential barrier is small enough for the particle to transition from well 4 to well 3. Right: The particle is now in potential well 3.

focal region while detecting the back reflected intensity on a photodiode (PD2). A polarization maintaining single-mode fiber (PMSM) acts as a spatial filter, such that the signal on PD2 peaks when the membrane surface coincides with the focal plane.

III. MEASUREMENT OF TRAPPING POTENTIAL

In order to investigate the optical trapping potential in close proximity of the SiN membrane, we measure the particle dynamics as a function of the distance between the membrane and the focal plane. To this end, at a pressure of 1.5 mbar, we move the membrane towards the objective at a speed of 20 nm/s, which is slow enough for the particle to thermalize at every position. During this approach, we record 600-ms-long time traces of the particle's motion on detector PD1 with a sampling rate of 667 kHz. From each time trace, we calculate the power spectral density $S_{VV}(\Omega)$ [23] and display the result in Fig. 2(a) as a false-color plot with d_{foc} on the horizontal axis and frequency Ω on the vertical axis. We observe salient dark regions in Fig. 2(a), corresponding to a strong peak in the power spectrum, which undergoes periodic frequency shifts between 50 and 150 kHz as the focus-to-surface distance d_{foc} is reduced down to about 2 μm. We attribute this strong peak to the particle's center-of-mass oscillation mode along the optical axis z. For even smaller values of d_{foc}, this strong peak shows an overall shift towards higher frequencies, exceeding 250 kHz as d_{foc} goes towards zero. Notably, at certain values of d_{foc}, the peak position jumps (e.g., at $d_{foc} = 1.1$ μm). Furthermore, we observe two less pronounced features [around $\Omega_x/(2\pi) = 150$ kHz and $\Omega_y/(2\pi) = 170$ kHz for $d_{foc} = 4$ μm], which correspond to the motion of the x and y modes, showing up on the z detector due to inevitably imperfect alignment. The oscillation frequency of the y mode exceeds that of the x mode due to the weaker confinement of the optical focus along the polarization direction of the field. All modes are thermally populated by collisions of the particle with gas molecules in the vacuum chamber. Importantly, the mode frequencies

Ω_x, Ω_y, Ω_z are a direct measure of the curvature of the trapping potential confining the particle.

We can intuitively understand the experimentally observed variation of the trap frequency with the approaching membrane by considering the intensity distribution of an optical beam strongly focused onto a dielectric membrane [24]. The interaction of the trapped particle with the optical field is dominated by the gradient force. The interference of the incoming trapping beam with its back reflection from the membrane generates a standing wave in front of the membrane. Field intensity I and optical potential U are linked by the equation $U = -\alpha' I/(2c\varepsilon_0)$ [5], where α' is the real part of the particle's polarizability, c is the speed of light, and ε_0 is the vacuum permittivity. These back reflections therefore modulate the trapping potential and several local optical potential minima form in front of the membrane, which we number starting with 1 for the first intensity maximum closest to the membrane. In Fig. 2(b), we schematically illustrate the typical behavior of both the optical potential and the particle as the membrane approaches. The particle resides in one potential minimum whose curvature depends on the exact membrane position and determines the oscillation frequency of the particle. In the example illustrated in Fig. 2(b), the particle is initially in well 4 (left panel). As the membrane is moved closer to the focal plane, the standing-wave pattern is shifted through the region of strongest lateral confinement of the beam and the particle is moved along with the standing-wave pattern towards the objective. With the membrane moving closer, the barrier between adjacent wells becomes small enough compared to the thermal energy for the particle to transition into the next well towards the membrane. This transition is depicted in Fig. 2(b) (middle panel), where the particle transitions from well 4 to well 3. As the membrane approaches even further [Fig. 2(b), right panel], the particle is carried along with the standing wave, until it again transitions to the next well. Accordingly, as we approach the membrane towards the focal plane, the particle is "handed" from well to well, leading to the periodic modulation of its oscillation frequencies observed in Fig. 2(a) [19,20]. The boxed numbers in Fig. 2(a) indicate the number of the well the particle resides in as the membrane approaches. The strong increase of the oscillation frequency Ω_z for distances d_{foc} smaller than 1 μm is explained by the stronger localization of the reflected field as the membrane enters the focal region of the field. This explanation is supported by the fact that the length scale on which the frequency Ω_z is strongly increased corresponds to the Rayleigh length of the laser focus, which is around 1 μm. In addition, we note that Ω_x and Ω_y decrease significantly for d_{foc} smaller than 0.8 μm. We explain this behavior by the widening of the potential along the transverse directions as well 1 is pushed away from the geometrical focus. Furthermore, we observe a spectral feature at 250 kHz in Fig. 2(a) crossing the z mode around $d_{\mathrm{foc}} \approx 0.2$ μm. This feature is the second harmonic of Ω_x and weakly couples to the z motion, which can be explained by nonlinearities of the optical potential sampled by the particle at room temperature [25].

We proceed with characterizing the optical potential shape at a given membrane position. To this end, we position the membrane at a fixed focus-to-surface distance and record a 60-s-long time trace of the particle's position along z at 1.5 mbar.

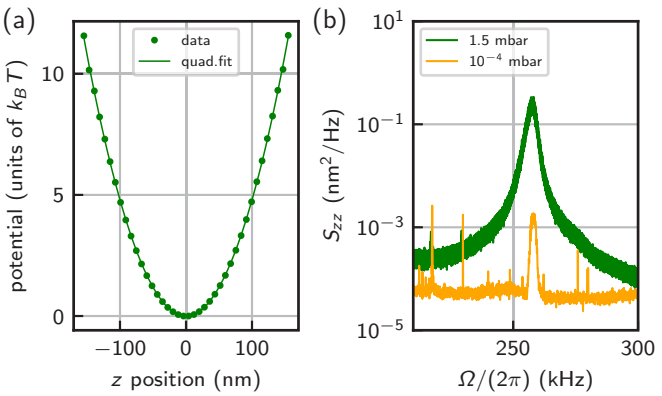

FIG. 3. (a) Reconstruction of the optical potential along z from a 60-s-long time trace of the particle motion recorded at 1.5 mbar, for $d_{\mathrm{foc}} = 390$ nm, and assuming a Boltzmann distribution of the particle positions (green data points). The green line shows a quadratic fit to the data. (b) Power spectral density S_{zz} recorded at $p = 1.5$ mbar without feedback cooling (green) and at $p = 10^{-4}$ mbar, where the particle's motion has been feedback cooled to 1 K (orange).

Assuming a Boltzmann distribution for the particle position $p(z) \propto e^{-U(z)/k_{\mathrm{B}}T}$ [26], where $p(z)$ is the probability density to find the particle at position z, we reconstruct the optical potential profile $U(z)$ probed by the particle along the z axis, as shown in Fig. 3(a) for $d_{\mathrm{foc}} = 390$ nm. The data are in excellent agreement with a parabolic fit [green line in Fig. 3(a)], such that the particle is well described as a harmonic oscillator.

IV. FEEDBACK COOLING

Having characterized the optical potential in front of the membrane using the particle as a probe, we turn to controlling the particle's center-of-mass motion using parametric feedback cooling [5,8]. With the particle trapped in well 1 in front of the membrane at a pressure of 1×10^{-4} mbar, we use the measurement record of the particle motion to derive a feedback signal, which we apply to the EOM to modulate the laser intensity in order to cool the particle's motion. The power spectral density of the cooled particle is plotted in orange in Fig. 3(b). For comparison, we also plot the power spectral density of the uncooled particle at a pressure of 1.5 mbar [green line in Fig. 3(b)]. With the center-of-mass temperature of the particle being proportional to the integrated power spectral density, we calculate a temperature of 1 K for the cooled oscillator. We note that the cooling performance is currently limited by the vacuum pressures reachable with our experimental setup.

V. MEASUREMENT OF PARTICLE-TO-SURFACE DISTANCE

Thus far, we have characterized the potential landscape in front of the dielectric membrane as a function of membrane position d_{foc}, measured relative to the focal plane of the objective. We now turn to a measurement of the distance d_{part} between the levitated nanoparticle and the membrane surface. For this measurement, we illuminate the particle from the side with a linearly polarized green probe laser at

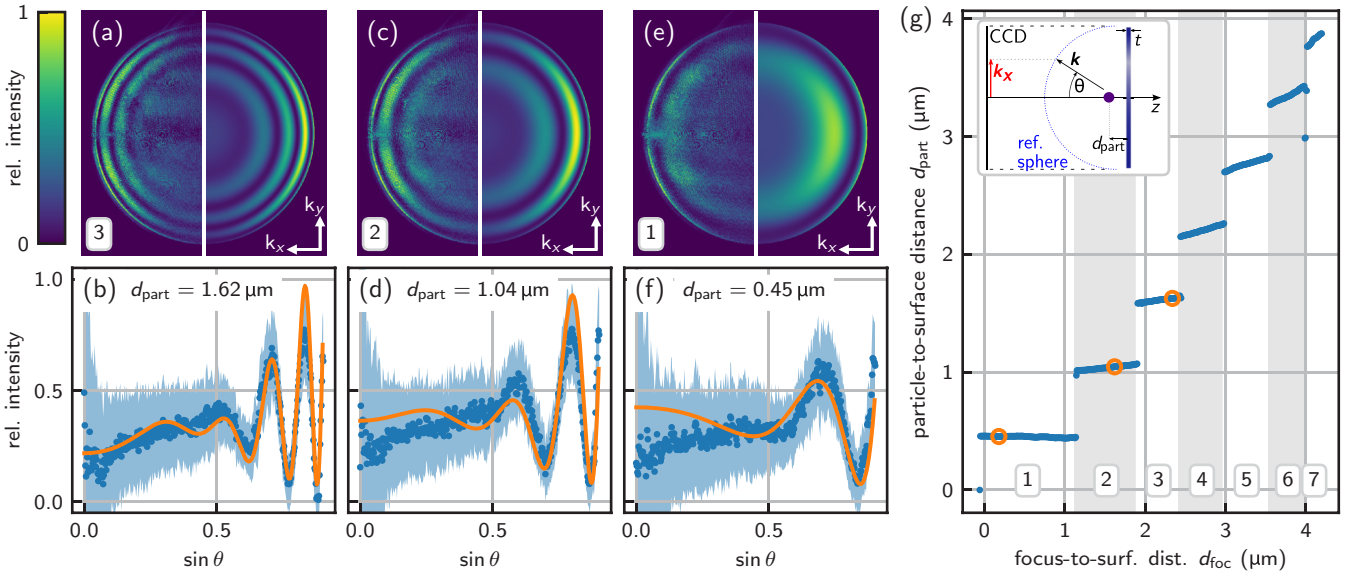

FIG. 4. Back focal plane imaging of a nanoparticle levitated in front of a SiN membrane (k_x and k_y denote the in-plane components of the wave vector). The scattering angle θ relative to the optical axis is given by $k\sin(\theta) = \sqrt{k_x^2 + k_y^2}$ [see inset in (g)]. (a) Left half: Image of the back focal plane measured at $d_{foc} = 2.34$ μm. Right half: Calculated back focal plane intensity distribution for a scatterer levitated at a distance $d_{part} = 1.62$ μm [extracted from the fit in (b)]. (b) Radially averaged intensity profile (blue points) from the measured image in (a). The blue shaded area corresponds to the experimental standard deviation. We fit (orange curve) the intensity profile according to our model, from which we extract the distance between the scatterer and the reflecting surface, $d_{part} = 1.62$ μm. (c)–(f) Analog to (a),(b) but for images recorded with particle in wells (c),(d) 2 and (e),(f) 1 [see Fig. 2(a)]. (g) Plot of the focus-to-surface distance d_{foc} vs the particle-to-surface distance d_{part}. The values for d_{part} are obtained by fitting the back focal plane images recorded during the entire approach of the membrane. The orange circles indicate the three examples detailed in (a), (c), and (e).

532 nm [see Fig. 1(a)]. Importantly, we carefully checked that switching on the green probe laser has no measurable influence on the particle dynamics. The probe field collected by the objective corresponds to the superposition of the field scattered by the particle directly into the objective and the scattered field reflected by the membrane towards the objective, similar to spectral self-interference microscopy [27]. The phase difference between these two fields depends on the radiation angle θ and leads to a characteristic interference pattern in the back focal plane of the objective [28]. This interference pattern provides a means to gauge the distance between the particle and the interface. With a dichroic mirror [DM in Fig. 1(a)], we separate the green light from the trapping light and image the back focal plane of the objective onto a camera. In Fig. 4(a) (left half), we show a back focal plane image recorded for $d_{foc} = 2.34$ μm, where the particle is in well 3. Note that the displacement from the center of the ring pattern is proportional to the transverse wave vector $k\sin(\theta)$, and the radius of the outermost ring is given by the numerical aperture $\mathrm{NA} = \sin(\theta_{max}) = 0.9$ of the objective with which the light is collected. We observe the dipolar radiation pattern of the point scatterer, modulated with a characteristic ring pattern, which encodes the distance between the particle and the surface, d_{part}. The distance d_{part} corresponds roughly to the number of fringes (interference undulations) multiplied by $\lambda/2$. To extract d_{part} more accurately, we radially average the measured intensity distribution in the back focal plane [blue data points in Fig. 4(b)] and fit the resulting intensity profile with the theory described in Ref. [29]. For our calculation, we take into account the thermal motion of the particle in the optical potential by performing a correspondingly weighted average of the back focal plane images for the values of d_{part} sampled by the particle. We obtain the best fit to our measurement for $d_{part} = [1.62 \pm 0.05(\mathrm{sys}) \pm 0.0002(\mathrm{stat})]$ μm, shown as the orange line in Fig. 4(b). We estimate the systematic error on d_{part} based on the residuals from the fit. The statistical error is estimated by evaluating the distance d_{part} from repeated measurements at the same membrane position, and amounts to 0.2 nm. For visual comparison, we show the corresponding theoretical back focal plane image in the right half of Fig. 4(a).

We display two more back focal plane images for $d_{foc} = 1.62$ μm [Fig. 4(c), particle in well 2] and $d_{foc} = 0.18$ μm [Fig. 4(d), particle in well 1]. Our analysis of the averaged intensity profiles shown in Figs. 4(d) and 4(f) yields the values $d_{part} = (1.04 \pm 0.05)$ μm (well 2) and (450 ± 50) nm (well 1), respectively. Since our particle is of nominal radius 68 nm, we deduce a minimum net distance between the surface of the particle and the membrane of 380 nm.

We note that besides the overall power and the particle-to-surface distance d_{part}, the only free parameter of the fit is the membrane thickness t. We consistently extract a value $t = (516 \pm 1)$ nm, which lies within the tolerance range provided by the manufacturer [(500 ± 25) nm].

With our interferometric measurement technique, by collecting a back focal plane image at every position d_{foc} of the approaching membrane, we can continuously monitor the particle-to-surface distance d_{part}, as shown in Fig. 4(g). The orange circles indicate the positions at which the three images displayed in Figs. 4(a), 4(c) and 4(e) were recorded. We note that the discrete steps in d_{part} coincide with the discontinuities

of the oscillation frequencies observed in Fig. 2(a) since both effects arise from the fact that the particle transitions into a neighboring well. This explanation is further supported by the observation that the step size in d_{part} observed in Fig. 4(g) is approximately $\lambda/2$, which corresponds to the spacing of the intensity maxima in a standing wave. We furthermore note that this step size increases for small d_{foc}, a feature that we attribute to the additional Gouy phase that is acquired near the focus.

Finally, we turn to the separation of well 1 from the membrane surface, which is 450 nm in the dataset presented in Fig. 4(g). We note that this separation is set by the complex reflection coefficient of the dielectric membrane and depends on both the membrane thickness and refractive index [30]. Therefore, by varying the membrane thickness, it is possible to adjust the separation of well 1 from the membrane surface.

VI. CONCLUSION

In summary, we have optically levitated a silica nanoparticle at a subwavelength surface-to-surface distance of 380 nm from a SiN membrane. By analyzing the particle's motion, we have characterized the trapping potential close to the dielectric interface. With an independent interferometric technique, we have measured the exact distance between the particle and the surface of the membrane. Furthermore, we have demonstrated feedback cooling of a nanoparticle levitated in subwavelength proximity of a dielectric membrane.

Looking ahead, the presented results match the requirements to harness the force sensitivity of levitated optomechanics for the characterization of short-range interactions. Such interactions include Casimir forces, noncontact friction, and, ultimately, non-Newtonian gravity [17,31,32]. Moreover, our technique brings measurements of thermal transfer dynamics at the nanoscale within reach [33]. To measure Casimir interactions, we envision to use a static-force-sensing scheme involving a free-falling particle [18]. This scheme requires one to prepare the nanoparticle in high vacuum (to minimize collisions with residual gas molecules) in a state of low center-of-mass temperature (to minimize the initial momentum before the free fall). The minimal static force that has been measured with this free-fall technique is 10 aN, while we estimate a Casimir force of 70 aN for a 136-nm-diameter nanoparticle residing in the first potential well [17]. Even the force of 1 aN expected in the second well seems accessible with this measurement protocol. Accordingly, we expect that our work will enable the investigation of Casimir interactions of a nanoparticle at distances comparable to the particle size. In such an experiment, it will be convenient to continuously tune the separation of the closest potential well relative to the membrane. To this end, we suggest the use of a counterpropagating phase-locked laser beam to create a conveyor belt in the focal region governed by the interference of the trapping beam, the field reflected from the membrane, and the counterpropagating beam [34]. In this configuration, tuning the relative phase between the trapping and counterpropagating beam provides a means to smoothly adjust the position of well 1 along the optical axis.

Finally, we also consider our work as a step towards on-chip levitated-optomechanical devices based on the combination of a levitated nanoparticle with integrated optics [15,35–37]. The use of a suspended silicon-nitride membrane provides the platform for approaching a wave guide structure to the particle that can be used to sense and control the particle position [30]. Such an on-chip integration would ultimately enable leveraging the sensitivity of optically levitated sensors for technological applications reaching beyond fundamental scientific investigations.

Note added. We have recently become aware of related work on the interaction of a levitated nanoparticle with a photonic crystal [38].

ACKNOWLEDGMENTS

The authors thank J. Gieseler and D. Windey for fruitful scientific discussions. This research was supported by ERC-QMES (Grant No. 338763) and the Swiss National Science Foundation through the NCCR-QSIT program (Grant No. 51NF40-160591).

[1] Z.-Q. Yin, A. Geraci, and T. Li, Int. J. Mod. Phys. B **27**, 1330018 (2013).
[2] O. Romero-Isart, M. L. Juan, R. Quidant, and J. I. Cirac, New J. Phys. **12**, 033015 (2010).
[3] M. Aspelmeyer, T. J. Kippenberg, and F. Marquardt, Rev. Mod. Phys. **86**, 1391 (2014).
[4] T. Li, S. Kheifets, and M. G. Raizen, Nat. Phys. **7**, 527 (2011).
[5] J. Gieseler, B. Deutsch, R. Quidant, and L. Novotny, Phys. Rev. Lett. **109**, 103603 (2012).
[6] N. Kiesel, F. Blaser, U. Delic, D. Grass, R. Kaltenbaek, and M. Aspelmeyer, Proc. Natl. Acad. Sci. USA **110**, 14180 (2013).
[7] J. Millen, P. Z. G. Fonseca, T. Mavrogordatos, T. S. Monteiro, and P. F. Barker, Phys. Rev. Lett. **114**, 123602 (2015).
[8] V. Jain, J. Gieseler, C. Moritz, C. Dellago, R. Quidant, and L. Novotny, Phys. Rev. Lett. **116**, 243601 (2016).
[9] G. Ranjit, M. Cunningham, K. Casey, and A. A. Geraci, Phys. Rev. A **93**, 053801 (2016).
[10] M. Armano *et al.*, Phys. Rev. Lett. **116**, 231101 (2016).
[11] D. Hempston, J. Vovrosh, M. Toroš, G. Winstone, M. Rashid, and H. Ulbricht, Appl. Phys. Lett. **111**, 133111 (2017).
[12] F. Monteiro, S. Ghosh, A. G. Fine, and D. C. Moore, Phys. Rev. A **96**, 063841 (2017).
[13] J. M. Obrecht, R. J. Wild, M. Antezza, L. P. Pitaevskii, S. Stringari, and E. A. Cornell, Phys. Rev. Lett. **98**, 063201 (2007).
[14] A. Arvanitaki and A. A. Geraci, Phys. Rev. Lett. **110**, 071105 (2013).
[15] P. Schein, P. Kang, D. O'Dell, and D. Erickson, Nano Lett. **15**, 1414 (2015).
[16] G. Winstone, M. Rademacher, R. Bennett, S. Buhmann, and H. Ulbricht, arXiv:1712.01426.
[17] A. A. Geraci, S. B. Papp, and J. Kitching, Phys. Rev. Lett. **105**, 101101 (2010).
[18] E. Hebestreit, M. Frimmer, R. Reimann, and L. Novotny, arXiv:1801.01169 [Phys. Rev. Lett. (to be published)].

[19] A. Jonáš, P. Zemánek, and E.-L. Florin, Opt. Lett. **26**, 1466 (2001).
[20] S. I. Ueda, M. Michihata, T. Hayashi, and Y. Takaya, Int. J. Optomechatron. **9**, 131 (2015).
[21] M. Frimmer, K. Luszcz, S. Ferreiro, V. Jain, E. Hebestreit, and L. Novotny, Phys. Rev. A **95**, 061801 (2017).
[22] M. Brownnutt, M. Kumph, P. Rabl, and R. Blatt, Rev. Mod. Phys. **87**, 1419 (2015).
[23] A. A. Clerk, M. H. Devoret, S. M. Girvin, F. Marquardt, and R. J. Schoelkopf, Rev. Mod. Phys. **82**, 1155 (2010).
[24] L. Novotny and B. Hecht, *Principles of Nano-Optics*, 2nd ed. (Cambridge University Press, Cambridge, 2012), pp. 70–74.
[25] J. Gieseler, L. Novotny, and R. Quidant, Nat. Phys. **9**, 806 (2013).
[26] L. Landau and E. Lifshitz, in *Statistical Physics*, 3rd ed., edited by L. Landau and E. Lifshitz (Butterworth-Heinemann, Oxford, 1980), pp. 79–110.
[27] B. J. Davis, M. Dogan, B. B. Goldberg, W. C. Karl, M. S. Ünlü, and A. K. Swan, J. Opt. Soc. Am. A **24**, 3762 (2007).
[28] L. Dai, I. Gregor, I. von der Hocht, T. Ruckstuhl, and J. Enderlein, Opt. Express **13**, 9409 (2005).
[29] L. Novotny and B. Hecht, *Principles of Nano-Optics*, 2nd ed. (Cambridge University Press, Cambridge, 2012), pp. 321–328.
[30] J. D. Thompson, T. G. Tiecke, N. P. de Leon, J. Feist, A. V. Akimov, M. Gullans, A. S. Zibrov, V. Vuletic, and M. D. Lukin, Science **340**, 1202 (2013).
[31] A. Almasi, P. Brax, D. Iannuzzi, and R. I. P. Sedmik, Phys. Rev. D **91**, 102002 (2015).
[32] J. L. Garrett, D. A. T. Somers, and J. N. Munday, Phys. Rev. Lett. **120**, 040401 (2018).
[33] M. Tschikin, S.-A. Biehs, F. Rosa, and P. Ben-Abdallah, Eur. Phys. J. B **85**, 233 (2012).
[34] D. Schrader, S. Kuhr, W. Alt, M. Müller, V. Gomer, and D. Meschede, Appl. Phys. B: Lasers Opt. **73**, 819 (2001).
[35] D. O'Shea, C. Junge, J. Volz, and A. Rauschenbeutel, Phys. Rev. Lett. **111**, 193601 (2013).
[36] M. Daly, V. G. Truong, and S. N. Chormaic, Opt. Express **24**, 14470 (2016).
[37] B. S. Schmidt, A. H. Yang, D. Erickson, and M. Lipson, Opt. Express **15**, 14322 (2007).
[38] L. Magrini, R. A. Norte, R. Riedinger, I. Marinković, D. Grass, U. Delić, S. Gröblacher, S. Hong, and M. Aspelmeyer, arXiv:1804.06676.